# Structure and Dynamics of a Benzenedithiol Monolayer on a Au(111) Surface

**Yongsheng Leng,*,†,‡ David J. Keffer,§ and Peter T. Cummings†,‡**

*Department of Chemical Engineering, Vanderbilt University, Nashville, Tennessee 37235-1604, Chemical Sciences Division, Oak Ridge National Laboratory, Oak Ridge, Tennessee 37831-6110, and Department of Chemical Engineering, The University of Tennessee, Knoxville, Tennessee 37996-2200*

*Received: February 17, 2003; In Final Form: June 23, 2003*

We use the universal force field (UFF) developed by Rappé et al. (Rappé, A. K.; Casewit, C. J.; Colwell, K. S.; Goddard, W. A.; Skiff, W. M. *J. Am. Chem. Soc.* **1992**, *114*, 10024) and the specific classical potentials developed from ab initio calculations for Au−benzenedithiol (BDT) molecule interaction to perform molecular dynamics (MD) simulations of a BDT monolayer on an extended Au(111) surface. The simulation system consists of 100 BDT molecules and three rigid Au layers in a simulation box that is rhombic in the plane of the Au surface. A multiple time scale algorithm, the double-reversible reference system propagator algorithm (double RESPA) based on the Nosé−Hoover dynamics scheme, and the Ewald summation with a boundary correction term for the treatment of long-range electrostatic interactions in a 2-D slab have been incorporated into the simulation technique. We investigate the local bonding properties of Au−BDT contacts and molecular orientation distributions of BDT molecules. These results show that whereas different basis sets from ab initio calculations may generate different local bonding geometric parameters (the bond length, etc.) the packing structures of BDT molecules maintain approximately the same well-ordered herringbone structure with small peak differences in the probability distributions of global geometric parameters. The methodology developed here opens an avenue for classical simulations of a metal−molecule−metal complex in molecular electronics devices.

## I. Introduction

The possibility of building sophisticated electronic devices from individual molecules has recently been demonstrated with the use of advanced microfabrication and self-assembly techniques.[1−3] Current−voltage and conductance measurements of molecular junctions[4,5] spurred theoretical interest in the modeling of such molecular electronic devices,[6−11] which in turn provides interpretations and feedback to the experimental measurements and molecular electronics architectural design. It is now well established that the transport properties of metal−molecule−metal junctions strongly depend on the molecular conformations,[3,4,9] the temperature,[11] and the contact nature between organic molecules and electrodes (the chemical bonding property).[12,13] Therefore, a better understanding of the equilibrium properties of molecular devices is critical to further calculations of transport characteristics. This task, in principle, requires an iterative procedure that combines quantum (electronic structure) calculations and classical (molecular configuration) calculations. At the quantum level, significant progress has been made in the framework of density functional theory (DFT) to calculate metal−single-molecule−metal conductance.[6−9] However, in practice, the molecular configuration of organic molecules between electrodes and binding properties at the molecule−metal contacts are not known a priori, which may result in large uncertainties in the transport calculations.[7,14] Thus, molecular simulations of self-assembled monolayers (SAMs) are therefore necessary to provide such valuable information. Because the molecular configuration in the electronic device under zero bias is determined by the intra- and intermolecular interactions and by the binding properties at the organic molecule−metal interface, a good force field describing these interactions is crucial.

In this paper, we present molecular dynamics (MD) simulations of benzenedithiol (BDT) molecules on Au(111) surfaces. This prototypical system of arylthiol molecules sandwiched between two gold electrodes demonstrates the ability to switch between conducting and nonconducting configurations depending on an external applied voltage.[5] We concentrate here on the equilibrium structure and dynamical properties of BDT molecules adsorbed on one extended Au(111) surface at room temperature (298 K) (i.e., without the second electrode being introduced into the system and with one extra H atom attached to the top S atom in BDT). We will provide a full description of the force field and the development of the numerical algorithm in our MD simulations. All of the atomic species (C, H, S, and Au) in the simulations are treated explicitly. For the intra- and intermolecular interactions between BDT molecules and BDT−Au nonbonded interactions, we use the universal force field (UFF),[15] combined with electrostatic partial-charge interactions derived from Mulliken population analysis. For the BDT−Au bonded interactions, which play an important role in the nature of the binding between BDT molecules and the Au(111) surface, we use for the first time a group of specific bonding potentials developed from ab initio quantum mechanical calculations.[16−18] Although many ab initio calculations of methylthiolate ($CH_3S-$) on Au(111) showed that the binding of sulfur headgroups was either on the hcp or the fcc hollow sites,[19−21] recent density functional theory (DFT) calculations[22,23] also showed that the back-bonded sulfur atom preferred bridge or bridgelike sites, depending on the chemistry of tail groups.

* Corresponding author. E-mail: yongsheng.leng@vanderbilt.edu.
† Vanderbilt University.
‡ Oak Ridge National Laboratory.
§ The University of Tennessee.

10.1021/jp034405s CCC: $25.00 
Published on Web 10/04/2003

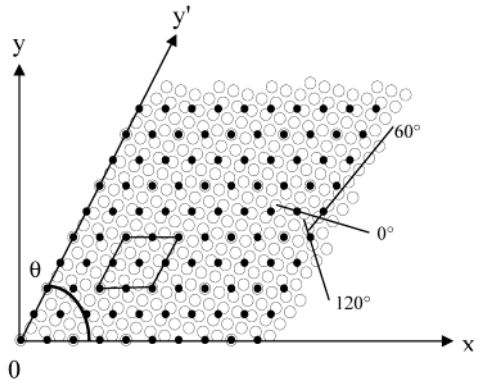


**Figure 1.** Rhombic simulation box of a BDT−Au system. The inset parallelogram shows a unit cell. ○, Gold atoms; ●, sulfur atoms. Three kinds of bridge sites, marked by 0, 60, and 120° lines, are also shown.

One possible reason is that the steric repulsions between the gold surface and the tail groups at these sites are lower than those at other sites.[22,23] This binding behavior has been confirmed for BDT−Au interactions from our recent ab initio calculations[16−18] (i.e., the binding site preference of BDT molecules on Au(111) is at the bridge sites rather than at the three-fold hollow sites). Furthermore, the DFT calculations from two basis sets (small and large) also show that the binding energies at the top and the hollow sites are comparable. These results are consistent with recent experimental measurements conducted by Wan et al.,[24] who used scanning tunneling microscopy (STM) to find that the benzenethiol (BT) molecules (we believe that BDT and BT molecules have the same binding properties on the Au(111) surface) adsorbed on the Au(111) surface formed a well-ordered monolayer with commensurate ($\sqrt{13} \times \sqrt{13}$) R13.9° symmetry. The unit cell contains four BT molecules, with one at the top site and the other three at the bridge sites.

On the basis of the experimental evidence and the specific ab initio calculations[16−18] for BDT−Au bonding, we construct our simulation system as shown in Figure 1. The MD simulation box consists of five replicas of the unit cell along both the $x$ and $y'$ directions, where $y'$ is the local skew axis. In the plane of the Au surface, this is a periodically replicated rhombic box containing 100 BDT molecules on a Au(111) surface. The geometric parameters of the unit cell are $a = b = \sqrt{13}a_{Au} = 10.38$ Å and $\theta = 60°$. The gold substrate is composed of three layers of static Au atoms with each layer containing 325 atoms. In Figure 1, only the top layer of gold atoms and adsorbed sulfur atoms are shown, with 4 BDT molecules (1 on the top site and the other 3 on the bridge sites) and 13 top-layer Au atoms in each unit cell. Periodic boundary conditions are imposed in the $x$ and the skew $y'$ directions.

The effect of the dynamics or relaxation of the gold substrate on the S−Au bonding property and molecular structure needs to be discussed. A recent DFT calculation for sulfur (S═), mercapto (HS−), and methylthiolate ($CH_3S-$) on Au(111) showed that upon the relaxation of the surface the binding potential energies changed only slightly.[23] Furthermore, simulations of alkylthiolate on Au(111) also showed that even though the first two layers of surface atoms undergo a significant relaxation at room temperature the packing structure of the monolayer still maintained ($\sqrt{3} \times \sqrt{3}$) R30° symmetry.[25] For the BDT−Au system, the impact of the dynamics of the gold substrate on the packing structure of BDT molecules will be investigated in our future work.

We first give detailed descriptions of the force fields, followed by the development of the MD simulation algorithm. To integrate precisely the dynamic equations for all of the particles, particularly for the light H atoms, we developed a double-reversible multi-time-scale algorithm originally proposed by Tuckerman et al.[26] (the reversible reference system propagator algorithm (r-RESPA)). In the subsequent section, we discuss the treatment of long-range electrostatic interactions. We find that for the 2-D rhombic simulation box the 3-D Ewald summation with the correction term (EW3DC) proposed by Yeh and Berkowitz[27] is still accurate. In the last section, we show the equilibrium structure and dynamic properties of BDT molecules on a Au(111) surface. The calculations involve the use of two sets of classical potential parameters derived from two DFT basis sets for BDT−Au bonding. Our simulations reveal that although the local geometric parameters for the BDT−Au bonding are different the global packing structures of BDT molecules maintained a similar well-ordered herringbone structure. The peak differences in the density distributions of global geometric parameters are within 15%.

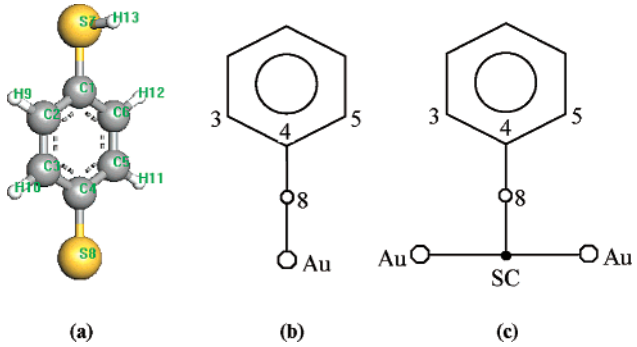


**Figure 2.** (a) Optimized BDT molecule, (b) on-top bonding, and (c) on-bridge bonding. SC represents a pseudoatom that is the site center of two bridge Au atoms.

## II. Force Fields

**A. Universal Force Field (UFF) for the BDT Organic Molecules.[15]** The universal force field (UFF) developed by Rappé et al.[15] has been parametrized for the full periodic table. The set of fundamental parameters is based only on the element, its hybridization, and connectivity. In this force field, the potential energy for a molecule is written as a superposition of various two-body, three-body, and four-body interactions. For the BDT molecule shown in Figure 2a, which is in an optimized structure obtained from the UFF, the potential energy is expressed as a sum of valence or bonded interactions and nonbonded interactions:

$$E = E_R + E_\theta + E_\phi + E_\omega + E_{vdw} + E_{el} \qquad (2\text{-}1)$$

The bonded interactions consist of bond stretching ($E_R$), angular distortions (i.e., bond angle bending ($E_\theta$), dihedral angle torsion ($E_\phi$), and inversion ($E_\omega$)). The nonbonded interactions consist of van der Waals ($E_{vdw}$) and electrostatic ($E_{el}$) terms. When we calculate the parameters in these interaction terms, the atomic types of C, H, and S in BDT molecules are C_R (resonant carbon), H_, and S_3+2 (tetrahedral sulfur in a +2 oxidation state). These energy terms are given below.

*1. Bond Stretching.* For two atomic species $I$ and $J$ bonded together, the harmonic potential is used to describe the bond vibrations:

$$E_R = \frac{1}{2}k_{IJ}(r - r_{IJ})^2 \qquad (2\text{-}2)$$

**TABLE 1: Potential Parameters in UFF**

| bond stretching | $r_{IJ}$ (Å) | $k_{IJ}$ (kcal/mol·Å$^2$) |
|---|---|---|
| C_R−C_R | 1.379 | 925.83 |
| C_R−H_ | 1.085 | 708.61 |
| C_R−S_3+2 | 1.800 | 588.45 |
| S_3+2−H_ | 1.429 | 438.3 |
| **angle bending** | $\theta_0$ (°) | $k_{IJK}$ (kcal/mol·rad$^2$) |
| C_R−C_R−C_R | 120 | 222.72 |
| C_R−C_R−H_ | 120 | 114.23 |
| C_R−C_R−S_3+2 | 120 | 201.01 |
| C_R−S_3+2−H_ | 92.1 | 102.16 |
| **torsion** | $\phi_o$ (°) | $1/2V_\phi$ (kcal/mol) |
| X−C_R−C_R−X | 180 (0) | 13.474 |
| X−C_R−S_3+2−X | 90 | 3.9528 |
| **inversion** | $\omega_0$ (°) | $k_{IJKL}$ (kcal/mol) |
| —C_R— | 0 | 6 |

where $r_{IJ}$ is the equilibrium bond length and $k_{IJ}$ is the bond-stretching force constants.

*2. Bond Angle Bending.* For two atoms *I* and *K* bonded to atom *J* in a general nonlinear case, the bond angle bending energy takes the form

$$E_\theta = \frac{k_{IJK}}{2\sin^2\theta_0}(\cos\theta - \cos\theta_0)^2 \qquad (2\text{-}3)$$

where $\theta_0$ is the equilibrium bond angle and $k_{IJK}$ is the angle-bending force constant.

*3. Torsion.* For two bonds *I J* and *KL* connected to a central bond *JK*, the torsion energy $E_\phi$ is given by

$$E_\phi = \frac{1}{2}V_\phi[1 - \cos n\phi_0 \cos n\phi] \qquad (2\text{-}4)$$

where $V_\phi$ is the rotational barrier, *n* is the periodicity of the potential, and $\phi_0$ is the equilibrium angle. There are two kinds of central bonds in the BDT molecule (Figure 2a). For the −C_R−C_R− central bond (*J* = an sp$^2$ center and *K* = an sp$^2$ center), $n = 2$ and $\phi_0 = 180$ or 0°. For the −C_R−S_3+2− central bond (*J* = an sp$^2$ center and *K* = an sp$^3$ center of the oxygen column), $n = 2$ and $\phi_0 = 90°$. When calculating torsion energies related to a given central bond *J*−*K*, all torsions about this bond should be considered, with each rotational barrier being divided by the number of torsions present about this *J*−*K* bond.

*4. Inversion.* When atom *I* is bonded exactly to three other atoms *J*, *K*, and *L*, the inversion energy is

$$E_\omega = k_{IJKL}(1 - \cos\omega_{IJKL}) \qquad (2\text{-}5)$$

where $k_{IJKL}$ is the force constant (kcal/mol) and $\omega_{IJKL}$ is the angle between the *IL* axis and the *IJK* plane. Similar to the torsion-energy calculation, for a given central atom *I*, all three axes (*IL*, *IJ*, and *IK*) should be considered, with each inversion barrier being divided by the number of inversions present (three) about the center *I*. For the BDT molecule in Figure 2a, inversion occurs at the six C_R atom bonding positions. The equilibrium inversion angle is 0°.

Table 1 lists all of the force constants and equilibrium values of bonded interactions.

*5. van der Waals Interactions.* For atoms in the same BDT molecule but separated by more than two neighboring atoms (the 1−2 and 1−3 interaction exclusions) or for atoms in different BDT molecules and all of the nonbonded Au atoms, the van der Waals interactions are included in the force field. A Lennard-Jones (L-J) 12−6-type expression is used:

**TABLE 2: Atomic Mass and Lennard-Jones 12−6-Type Parameters in UFF**

| atom type | mass (amu) | $D_{II}$ (kcal/mol) | $x_{II}$ (Å) |
|---|---|---|---|
| C | 12.0000 | 0.1050 | 3.851 |
| H | 1.0000 | 0.044 | 2.886 |
| S | 32.0000 | 0.274 | 4.035 |
| Au | 197.0000 | 0.039 | 3.293 |

$$E_{vdw} = D_{IJ}\left[\left(\frac{x_{IJ}}{r}\right)^{12} - 2\left(\frac{x_{IJ}}{r}\right)^{6}\right] \qquad (2\text{-}6)$$

$D_{IJ}$ is the well depth in kcal/mol and $x_{IJ}$ is the van der Waals bond length in Å. For different atomic species interactions, the general $x_{IJ}$ and $D_{IJ}$ parameters are obtained from the homonuclear parameters using the geometric mean combination rule. Table 2 summarizes all of the L-J 12−6 potential parameters for C, H, S, and Au atomic species.

*6. Electrostatic Interactions.* The partial charges from Mulliken population analysis in ab initio calculations[16−18] are assigned to individual atoms in BDT molecules and bonded Au atoms. Similar to the treatment of van der Waals interactions, the convention of 1−2 and 1−3 exclusions also applies to the Coulombic interactions. A special treatment of long-range electrostatic interactions will be discussed in section IV.

**B. BDT−Au Bonding Potentials.** Following the general rules in the UFF, the bonded interactions between BDT molecules and the Au(111) surface are represented by a few Au atoms involved in chemical bonding.[16−18] For example, when a BDT molecule is on the top site of a Au(111) surface (Figure 2b), the bond stretching, bond angle bending, and bond torsion correspond to Au−S8, Au−S8−C4, and Au−S8−C4−C3. (Au−S8−C4−C5 is also considered by dividing the force constant by a factor of 2.) For BDT molecules adsorbed on the bridge and the three-fold hollow sites (this case is not considered here), we introduce a pseudoatom that represents the geometric site center (SC) of the bridge or hollow sites. The bond stretching, bond angle bending, and bond torsion in the on-bridge case correspond to SC−S8, SC−S8−C4, and SC−S8−C4−C3 (SC−S8−C4−C5) (Figure 2c). There is a second bond torsion introduced: Au−SC−S8−C4. This term determines the bending direction of BDT molecules relative to the orientation of Au sites. Interactions of BDT molecules with all of the other nonbonded Au atoms are treated as van der Waals interactions, as discussed in section II.A.5.

The functional forms of the BDT−Au bonding potentials are given as below.

*Bond Stretching*:

$$E_{x,r} = \frac{1}{2}k_{x,r}(r - r_{x,\min})^2 \qquad (2\text{-}7)$$

where $k_{x,r}$ and $r_{x,min}$ are the force constant and equilibrium distance. The subscript *x* can take on values of *T* and *B* for the on-top and on-bridge sites.

*Bond Angle Bending:*

$$E_{x,\theta} = \frac{1}{2}k_{x,\theta}(\theta - \theta_{x,\min})^2 \qquad (2\text{-}8)$$

where $k_{x,\theta}$ and $\theta_{x,\min}$ are the bending force constant and equilibrium angle.

**TABLE 3: Parameters in BDT−Au Bonding Potentials**

| | properties | units | small basis | large basis |
|---|---|---|---|---|
| top site | $r_{T,min}$ | Å | 2.538 | 2.335 |
| | $k_{T,r}$ | kcal/(mol·Å$^2$) | 152.84 | 255.42 |
| | $\theta_{T,min}$ | deg | 102 | 103 |
| | $k_{T,\theta}$ | kcal/(mol·rad$^2$) | 57.28 | 83.92 |
| | $\phi_{T,min}$ | deg | 90 | 90 |
| | $k_{T,\phi}$ | kcal/mol | 3.683 | 3.853 |
| bridge site | $r_{B,r}$ | Å | 2.350 | 2.075 |
| | $k_{B,r}$ | kcal/(mol·Å$^2$) | 74.62 | 49.3 |
| | $\theta_{B,min}$ | deg | 108 | 107.5 |
| | $k_{B,\theta}$ | kcal/(mol·rad$^2$) | 25.04 | 43.76 |
| | $\phi_{B,min}$ | deg | 90 | 90 |
| | $k_{B,\phi}$ | kcal/mol | 112.6 | 39.29 |
| | $\psi_{B,min}$ | deg | 0 | 0 |
| | $k_{B,\psi}$ | kcal/mol | 13.38 | 24.68 |

**TABLE 4: Mulliken Partial Charges[a]**

| elements | small basis | large basis |
|---|---|---|
| C1 | −0.29/−0.38 | −0.28/−0.49 |
| C2 | −0.17/−0.15 | −0.11/−0.06 |
| C3 | −0.17/−0.16 | −0.11/−0.12 |
| C4 | −0.34/−0.36 | −0.35/−0.49 |
| C5 | −0.17/−0.16 | −0.11/−0.12 |
| C6 | −0.17/−0.15 | −0.11/−0.06 |
| S7 | −0.09/−0.13 | −0.25/−0.09 |
| S8 | 0.02/0.21 | −0.07/0.23 |
| H9 | 0.24/0.25 | 0.22/0.23 |
| H10 | 0.25/0.25 | 0.22/0.22 |
| H11 | 0.25/0.25 | 0.22/0.22 |
| H12 | 0.24/0.25 | 0.22/0.23 |
| H13 | 0.3/0.3 | 0.37/0.3 |
| Au | 0.1/(−0.01) × 2 | 0.14/0.0 × 2 |

[a] On-top/on-bridge sites, unit = electron.

*Bond Torsion:*

$$E_{x,\phi} = \frac{1}{2}k_{x,\phi}[1 - \cos(n\phi_{x,\min})\cos(n\phi)] \qquad (2\text{-}9)$$

where $k_{x,\phi}$ and $\phi_{x,min}$ are rotational barrier and equilibrium angle. Equation 2-9 is also valid for the second torsion on the bridge site, with the subscript $\phi$ being replaced by $\psi$. Because the rotation of the benzene ring has 2-fold symmetry, the periodicity of the potential in eq 2-9 is 2 ($n = 2$).

Parameters in eqs 2-7−2-9 are fitted to ab initio total energy calculations using the NWChem package.[16] Two sets of parameters corresponding to the small and large basis sets in the density functional theory (DFT) calculations are listed in Table 3.[28,29] Distributions of the partial charges in the BDT molecule and the bonded Au atoms are listed in Table 4. These point charges are derived from the Mulliken population analysis in ab initio calculations.

## III. Algorithm

We find that BDT molecules are very "rigid" because of the high stiffness of the benzene ring and strong valence bonding. As a result, a brute-force molecular dynamics simulation would require a time step much shorter than 1 fs to simulate a system containing BDT molecules. Two time-scale problems are involved in the current BDT−Au molecular system. One is the fast variations with large magnitudes of intramolecular (short-range) forces versus the slow variations of intermolecular forces. The precise integration of the equations of motion of the particles needs a much smaller time step for the intramolecular (long-range) forces than for the intermolecular forces. Another issue is the disparate masses in the system: the H atoms are 1 order of magnitude lower in mass than other particles, thus they have much higher vibration frequencies (the fast degrees of freedom) than others. A multiple-time-scale method, the double-reversible RESPA (reference system propagator algorithms) based on the original work of Tuckerman et al.[26] and the extended system Nosé−Hoover dynamics[30,31] for the NVT ensemble has been constructed and applied to the BDT−Au system. Here, the conserved quantity (pseudo-Hamiltonian) of the system is

$$H'(x, p, \eta, p_\eta) = V(x) + \sum \frac{p^2}{2m} + \frac{p_\eta^2}{2Q} + 3NkT\eta = V + V_{kin} + V_{Nosé} \qquad (3\text{-}1)$$

where $x$ and $p$ are the positions and momenta of particles, $\eta$ and $p_\eta$ are the extended thermostat and conjugated momentum, $Q$ is the mass of the thermostat, $k$ is the Boltzmann constant, and $T$ is the temperature. In eq 3-1, variables $V$ and $V_{kin}$ are the potential and kinetic energies of molecular system; the last term, $V_{Nosé}$, can be recognized as the heat adsorbed by the external bath during the equilibration. Tuckerman et al. [26] showed that any integrators derived from Trotter factorization of the Liouville operator i$L$ are reversible. They then constructed a general double-RESPA scheme for the systems with short−long-range force separations and disparate mass problems. Because this double RESPA involves updates of the long-range forces in the inner loop for the light particles and the ratio of the number of H atoms to other heavy particles (C and S atoms in BDT) is $^5/_8$, we find that their method is not particularly efficient. We therefore constructed a slightly different scheme of double RESPA, which involves a further decomposition of the propagator for the light particles within the reference system. The CPU time used for this double RESPA is almost the same as that for the single RESPA because the updates of short-range forces are quite fast. We also investigated the Nosé−Hoover chain propagator[32,33] (with two thermostats), which was originally designed for small or stiff systems. We found that there was no improvement either in efficiency (increasing time step) or in stability. In the Appendix, the numerical procedure for the proposed double RESPA is presented in detail.

## IV. Treatment of Long-Range Coulombic Interactions

For a 2-D periodic system that has finite length in the third direction, an accurate 2-D Ewald summation (EW2D) technique had been given.[34−36] However, it is well known that EW2D is much more expensive than the 3-D Ewald summation (EW3D)[37,38] because of the double sum in reciprocal space.[39] Recently, Yeh and Berkowitz [27] proposed an efficient 2-D Ewald method that combines a general EW3D with a shape-dependent correction term introduced by Smith.[40] This method, called EW3DC, has a similar surface term in the standard Ewald formula[37,38] but with a different proportionality factor and involving only the $z$ component of the total dipole moment. This method is straightforward and can be easily incorporated into the standard EW3D algorithm. Because the accuracy of the EW3DC method has thus far been tested only for cubic simulation boxes with sufficient vacuum in the $z$ direction, one of our objectives in this paper is to evaluate the applicability of the method for a right rhombic prism simulation cell, such as that in Figure 1. For a general parallelogram-shaped simulation box, an exact EW2D has been given recently by Grzybowski and Brodka.[41] We will examine EW3DC on the basis of their calculations. Other treatments of 2-D Ewald summation, either using the plane-wave-based DFT[42] or an electrostatic layer correction,[43] have also been reported recently. The former is a

new reciprocal-space-based method that can be easily combined with SPME (smooth particle-method Ewald) summation and other novel approaches to study hybrid ab initio/molecular mechanics problems on surfaces. The latter is claimed as an extension of EW3DC and can give rigorous error estimates because of the image layers in the third direction. Implementing these two recent schemes is beyond the scope of this present paper. As we will see below, direct testing of EW3DC with regard to the specific right rhombic prism simulation cell and slab geometry of the BDT−Au molecular system shows that the current EW3DC method is sufficient in terms of accuracy and efficiency.

For molecular systems, as opposed to systems composed simply of point ions, an additional modification in the Ewald summation is necessary to correct for the excluded Coulombic interactions (here, the 1−2 and 1−3 intramolecular interactions in the BDT molecule and the bonded Au atom, as discussed in section II.A.6). These energy terms are simply subtracted from the standard Ewald sum and put together with the self-exclusion term as shown below. For a neutral molecular system, the total electrostatic energy is therefore given by the following equation:

$$E_{\mathrm{el}} = \frac{1}{2V_0\epsilon_0}\sum_{\underline{k}\neq 0}^{\infty}\frac{\exp(-k^2/4\alpha^2)}{k^2}\left|\sum_j^N q_j \exp(-\mathrm{i}\underline{k}\cdot\underline{r}_j)\right|^2 + \frac{1}{4\pi\epsilon_0}\sum_{n<j}^{N}\frac{q_j q_n}{r_{nj}}\mathrm{erfc}(\alpha r_{nj}) - \frac{1}{4\pi\epsilon_0}\sum_{\text{molecules}}\left[\frac{\alpha}{\sqrt{\pi}}\sum_{j=1}^{M} q_j^2 + \sum_{n,j}^{\text{list}}\frac{q_n q_j}{r_{nj}}\right] + \frac{M_z^2}{2V_0\epsilon_0} \quad (4\text{-}1)$$

In this equation, the first term is the reciprocal sum for all of the Gaussian charges ($N$), where $V_0$ is the volume of the simulation box, $\epsilon_0$ is the permittivity of free space, and $\alpha$ is the Ewald convergence parameter. The second term is the standard real-space sum, where erfc is the complementary error function. The third term is the self-exclusion plus those from 1−2 and 1−3 exclusions, where the number "list" contains all of the 1−2 and 1−3 exclusions within the molecule and $M$ is the total number of atoms in the molecule. The last term is the correction term from Yeh and Berkowitz,[27] which is obtained by the plane-wise summation method proposed by Smith,[40] where $M_z$ is the $z$ component of the total dipole moment of the simulation box. In the reciprocal sum of eq 4-1, $\underline{k}$ is a reciprocal lattice vector defined by

$$\underline{k} = k_x\underline{u} + k_y\underline{v} + k_z\underline{w} \quad (4\text{-}2)$$

where $k_x$, $k_y$, and $k_z$ are integers and $\underline{u}$, $\underline{v}$, and $\underline{w}$ are the reciprocal-space basis vectors. Both $V_0$ and $\underline{u}$, $\underline{v}$, and $\underline{w}$ are derived from the vectors ($\underline{a}$, $\underline{b}$, $\underline{c}$) defining the simulation box. Thus

$$V_0 = |\underline{a}\cdot\underline{b}\times\underline{c}| \quad (4\text{-}3)$$

and

$$\underline{u} = \frac{2\pi}{V_0}\underline{b}\times\underline{c} \qquad \underline{v} = \frac{2\pi}{V_0}\underline{c}\times\underline{a} \qquad \underline{w} = \frac{2\pi}{V_0}\underline{a}\times\underline{b} \quad (4\text{-}4)$$

In our BDT−Au molecular system, $\underline{a} = (L_x, 0, 0)$, $\underline{b} = (L_{y'}\cos\theta, L_{y'}\sin\theta, 0)$, and $\underline{c} = (0, 0, L_z)$, where $L_x$, $L_{y'}$, and $L_z$ are the rhombic box lengths and $\theta = 60°$ (Figure 1).

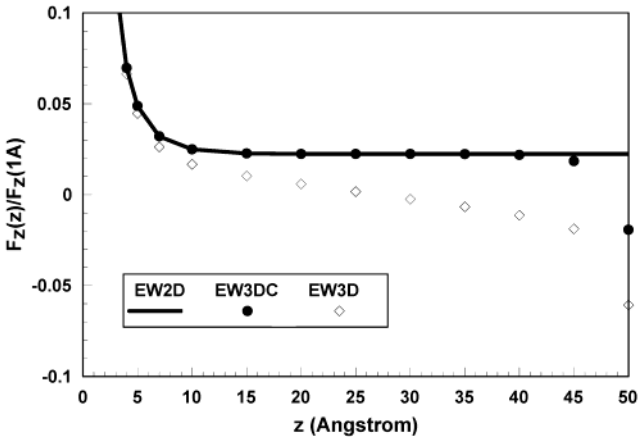


**Figure 3.** Comparisons of the $z$-component forces acting on the unit point charge at (0, 0, $z$) by another opposite unit charge fixed at (0, 0, 0) from different Ewald methods. The simulation box is rhombic. $L_x$ = 18 Å, $L_{y'}$ = 18 Å, and $L_z = 3L_x$. Reciprocal-space cutoff = 3.49 Å$^{-1}$, and convergence factor $\alpha$ = 0.45 Å$^{-1}$. Clearly, the results of EW3DC agree well with EW2D results until the distance $z$ is greater than 40 Å.

The force on an atom $j$ is obtained by differentiating eq 4-1 and is given by

$$F_{j\beta} = -\frac{\partial E_{\mathrm{el}}}{\partial r_{j\beta}} = \frac{q_j}{V_0\epsilon_0}\sum_k A_k k_\beta I_m(Q\mathrm{e}^{\mathrm{i}\underline{k}\cdot\underline{r}_j}) + \frac{q_j}{4\pi\epsilon_0}\sum_{n>j}^{N}\frac{q_n}{r_{jn}^3}(r_{j\beta}-r_{n\beta})\left[\mathrm{erfc}(\alpha r_{jn}) + \frac{2\alpha r_{jn}}{\sqrt{\pi}}\mathrm{e}^{-\alpha^2 r_{jn}^2}\right] - \frac{q_j}{4\pi\epsilon_0}\sum_{\text{molecules}}\sum_{n}^{\text{list}}\frac{q_n}{r_{jn}^3}(r_{j\beta}-r_{n\beta}) - \frac{q_j M_z}{V_0\epsilon_0}\delta_{z\beta} \quad (\beta = x, y, z) \quad (4\text{-}5)$$

where

$$A_k = \frac{\exp(-k^2/4\alpha^2)}{k^2}$$

and

$$k_\beta = k_x u_\beta + k_y v_\beta + k_z w_\beta$$

$$Q = \sum_n^N q_n \exp(-\mathrm{i}\underline{k}\cdot\underline{r}_n)$$

which is the total Gaussian charge.

To test the validity of the EW3DC for the right rhombic prism simulation box, we repeat Yeh and Berkowitz's calculations using Spohr's similar geometry[39] but with a noncubic cell. We calculated the $z$-component force between two opposite unit charges at (0, 0, 0) and (0, 0, $z$) using EW2D, EW3D, and EW3DC. Exact EW2D results are provided by Grzybowski and Brodka.[41] Geometric parameters of the box are $L_x = L_{y'}$ = 18Å, $L_z = 3L_x$ = 54 Å, and $\theta = 60°$; $\alpha$ = 0.45 Å$^{-1}$ and a reciprocal-space cutoff radius of 3.49 Å$^{-1}$ have been used. The results are shown in Figure 3. We see that the results for EW3DC agree well with EW2D results until the distance $z$ is greater than 40 Å. At this position, the empty space is only 14 Å, approximately one-third of the thickness of the charged layer. On the contrary, the results for EW3D show significant deviations from EW2D results because of the effects of unscreened image layers in the

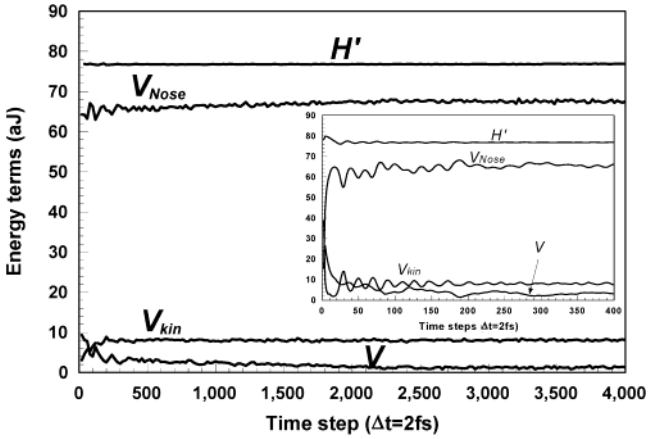


**Figure 4.** Equilibration of BDT molecules on a Au(111) surface during the first 8-ps MD run. The inset shows the first 0.8-ps relaxation process.

$z$ direction. The leveling off of the force $F_z$ at large $z$ ($>L_x = L_{y'}$) also shows that as the two point charges in a 2-D periodic system are sufficiently far apart in the $z$ direction their electrostatic interaction approaches that between two charged surfaces in a parallel plate capacitor.[39]

When calculating the electrostatic interactions using EW3DC for the BDT−Au molecular system, we note that in Figure 1 the lateral sizes of the simulation box are $L_x = L_{y'} = 51.9$ Å. Because the partial charges are distributed in BDT molecules and bonded Au atoms, the thickness of the charged layer in the normal direction is only about 9 Å, which is much smaller than its lateral dimensions. For this thin-slab geometry, the Smith planewise summation method,[40] which yields the correction term of eq 4-1,[27] is particularly suitable. We find that in this case it is not necessary to enlarge the size of the simulation box in the $z$ direction, $L_z$, to several times its lateral size, $L_x$. In fact, Figure 3 also shows that the height of the empty space does not have to be at least $1.5L_x$. We therefore select $L_z = 20$ Å, which is about 2 times the charged layer thickness and much less than $L_x$. Comparing with the case of $L_z = 2L_x = 103.8$ Å for the same reciprocal-space cutoff shows that they give the same particle forces and Ewald potential energy. The advantage of using a small $L_z$ is that the number of reciprocal-space $k$ vectors along the $z$ direction can be significantly decreased. In our MD simulations, the Ewald convergence parameter and reciprocal-space cutoff in the simulations are 0.3 and 1.8 Å$^{-1}$, respectively. The real-space summation follows the general rule of minimum image consideration (second term in eq 4-1), and a cutoff radius of $3\sigma$ has been used.

## V. Results and Discussion

**A. Equilibration.** Figure 4 shows the variations in the energy terms in eq 3-2 during the first 8-ps relaxation of BDT molecules on the Au(111) surface at 298 K. The first set of BDT−Au bonding potential parameters from Table 2 is used (small basis). The initial configuration of BDT molecules is arranged to be standing normal to the Au(111) surface. The time step in molecular dynamics is $\Delta t = 2$ fs. In implementing the double-RESPA scheme sketched in the Appendix, the numbers of inner and inner−inner loops are $n = 5$ and $m = 4$, so the gain is 20. The smallest time step is 0.1 fs for the H-atom motion. The mass of the thermostat $Q$ is chosen according to the equation $Q = 3NkT\tau$,[2,26] where $\tau$ is some characteristic time in the system. Here we arbitrarily choose $\tau = 10$ fs. The Figure clearly shows that the system approaches the equilibrium very quickly (i.e., in approximately 4 ps). The inset in Figure 4 shows a more refined relaxation process during the first 0.8 ps, where the huge unphysical configuration energy is adsorbed by the Nosé thermostat, $V_{\text{Nosé}}$, whereas the total quantity $H'$ remains constant (except for a small fluctuation in the first few time steps). The equilibrium molecular configuration of BDT molecules on a Au(111) surface is shown in Figure 5a. We see that the BDT molecules form a well-ordered herringbone structure along approximately the 120° direction relative to the $x$ axis. Detailed dynamics animation at room temperature reveals that the planar structure of the benzene rings is well maintained and that both the two S−C bonds and the four C−H bonds lie in the benzene-ring plane. The S−C−C bond angles fluctuate around 120° by about ±20°, and the H−C−C bond angles have even larger fluctuations (120 ± 30°). The hydrogen atoms (H13) bonded to sulfur atoms (S7) (Figure 2a) are excited basically in two vibration modes. One is the constraint rotation around the S7−C1 bond, and the other is the bending motion between the S7−C1 and S7−H13 bonds. A snapshot of these H atoms' positions is seen from the top view of the BDT molecular configuration in spacefill representation (Figure 5b). We note that in a recent molecular dynamics simulation of benzenethiol (BT) molecules on a Au(111) surface[44] using the CHARMM program a similar herringbone structure was obtained but the packing structure was $(\sqrt{3} \times \sqrt{3})30°$ and the BT−Au bonding potential was not well developed.

Calculations using the second set of BDT−Au bonding potential parameters from Table 2 (large basis) showed the same relaxation and dynamics properties of BDT molecules, but with a different total energy level $H'$. The same herringbone structure is also obtained. Below we give a detailed analysis of the local BDT−Au bonding and global geometric parameter distributions.

**B. BDT−Au Bonding Geometric Parameter Distributions.** In Table 3, we first notice that the top stretching force constants from the two basis sets are 152.84 and 255.42 kcal/(mol·Å$^2$) and that the bond lengths are 2.538 and 2.335 Å, respectively. These values are comparable to early theoretical predictions of the bonding between the S atom in an alkylthiol molecule and a flat gold surface (219.4 kcal/(mol·Å$^2$) and 2.4 Å).[45] The bridge-site force constants and distances (74.62 and 49.3 kcal/(mol·Å$^2$); 2.35 and 2.075 Å, respectively) are relatively low because S atoms sit over SC sites. Because the specific bond bending and torsion potentials from quantum chemistry calculations are also included in the current model, the newly developed Au−S bonding potentials are more accurate than the general isotropic potentials, which take into account only the Au−S binding distance.[45,46]

To investigate how the BDT−Au bonded interaction potentials dominate local bonding behavior, we plot the probability distributions for all of the bonding geometric parameters from MD simulations and the corresponding normalized Boltzmann factor distributions, which are solely determined by the specific potentials. Statistical averages were obtained over the next 12-ps run after the initial 8-ps equilibration. The time step is 2 fs, and the sampling interval is 30 fs.

The normalized Boltzmann factor is defined as

$$B = \frac{e^{-E(x)/k_B T}}{\int_0^\infty e^{-E(x)/k_B T} dx} \tag{5-1}$$

where $E(x)$ is the specific bonding energy from eqs 2-7−2-9 and $k_B$ is the Boltzmann constant.

Figure 6 shows the BDT−Au bond-stretching distributions on the top and bridge sites from the two basis sets. The bond-bending curves are shown in Figure 7. Whereas the small and

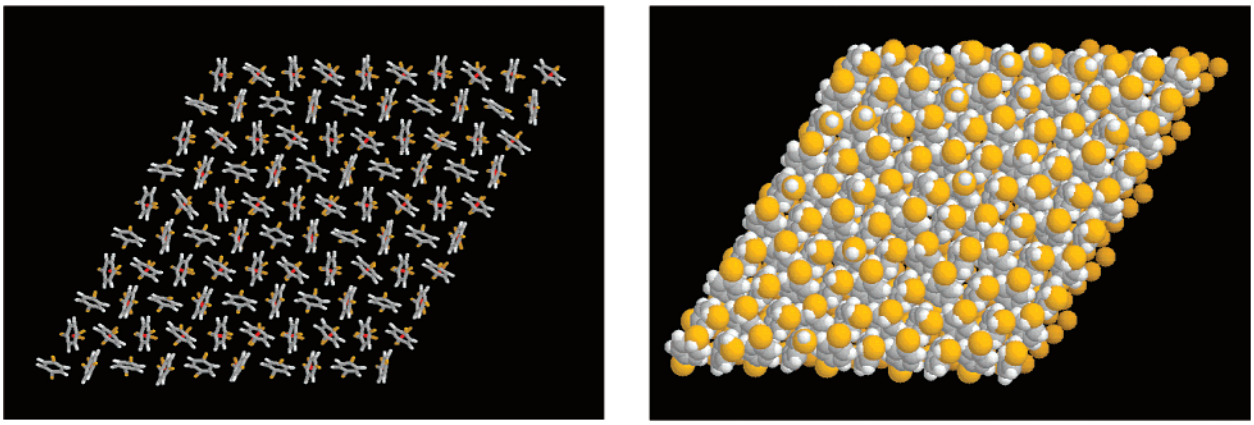

**Figure 5.** Packing structure of a BDT monolayer on a Au(111) surface. (a) Stick representation. The structure exhibits a herringbone pattern clearly visible along approximately the 120° direction. (b) Atoms shown in spacefill mode based on van der Waals radii. Bright yellow, S; deep yellow, Au, grey, C; white, H.

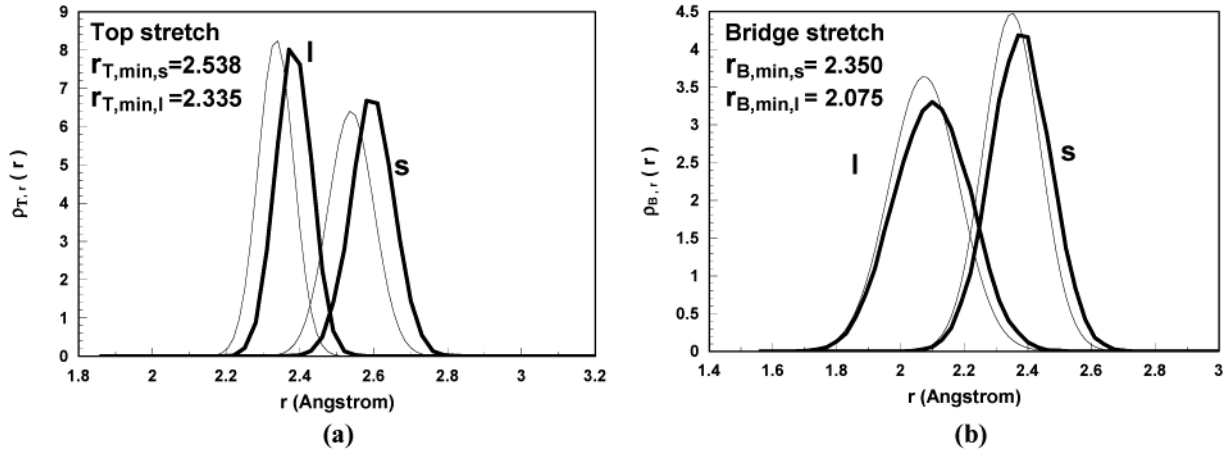


**Figure 6.** Normalized distributions of Au−S bond stretching. The dashed lines are the normalized Boltzmann distributions solely determined by the corresponding potentials (eq 2-16). Characters "l" and "s" represent results from large and small basis sets in ab initio calculations. Data were averaged over a 12-ps run with $\Delta t = 2$ fs. (a) Top site; (b) bridge site.

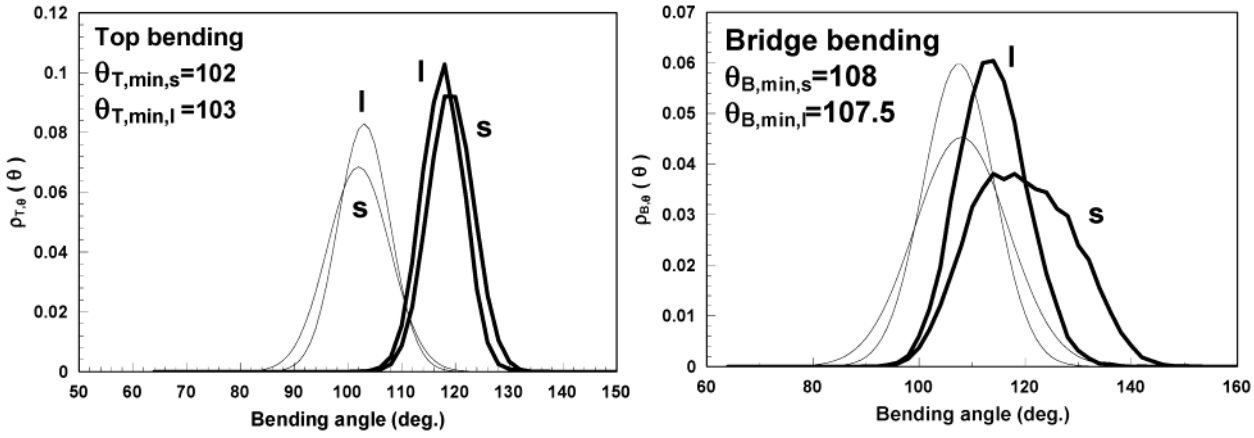


**Figure 7.** Normalized distributions of Au−S bond bending. The dashed lines are the normalized Boltzmann distributions solely determined by the corresponding potentials (eq 2-17). Characters "l" and "s" represent results from large and small basis sets in ab initio calculations. Data were averaged over a 12-ps run with $\Delta t = 2$ fs. (a) Top site; (b) bridge site.

large basis sets yield two different potential parameters (Table 3), the corresponding curves also fall into two different sets. In the Figures, the MD distribution curves on the top site depict significant shifts relative to their normalized Boltzmann distributions. When realizing that the original bonding potential is developed on the basis of only one or two bonded Au atoms, this phenomenon shows that the BDT−BDT and BDT−Au nonbonded interactions also play an important role in BDT−Au binding. For the bridge adsorption case, the shifts are relatively small, implying that BDT−Au bonding at these sites is dominant. Figures 6 and 7 also show that large force constants yields sharp distribution curves.

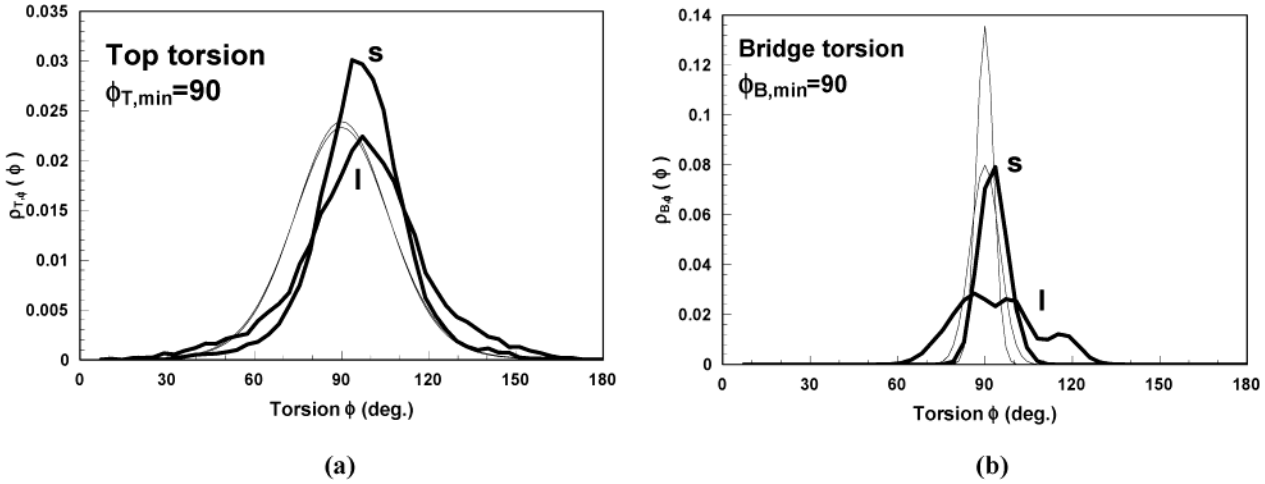


**Figure 8.** Normalized distributions of Au−S bond torsion. The dashed lines are the normalized Boltzmann distributions solely determined by the corresponding potentials (eq 2-18). Characters "l" and "s" represent results from large and small basis sets in ab initio calculations. Data were averaged over a 12-ps run with $\Delta t = 2$ fs. (a) Top site; (b) bridge site.

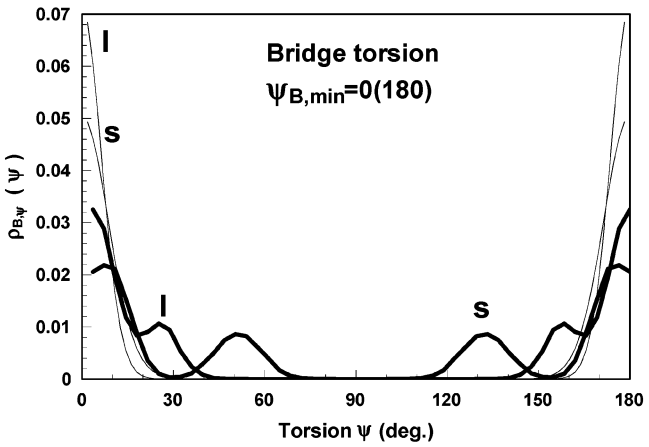


**Figure 9.** Normalized density distributions of the second torsion on a bridge site. The dashed lines are the normalized Boltzmann distributions solely determined by the corresponding potentials (eq 2-18). Characters "l" and "s" represent results from large and small basis sets in ab initio calculations. Data were averaged over a 12-ps run with $\Delta t = 2$ fs.

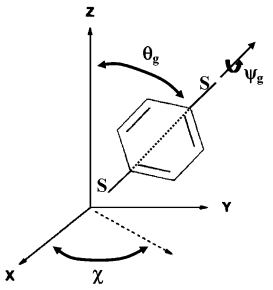


**Figure 10.** Global orientation parameters of the BDT molecule.

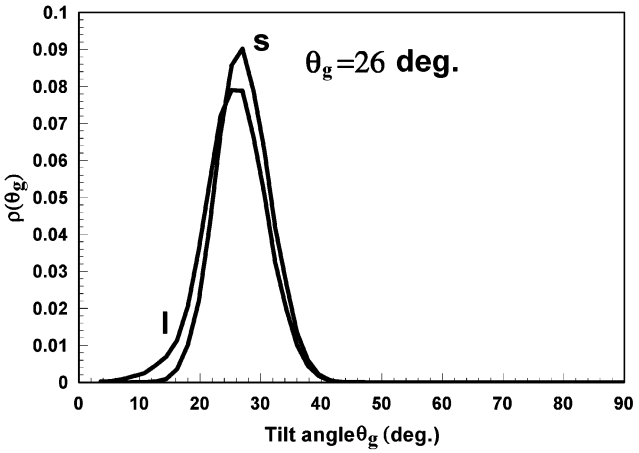


**Figure 11.** Normalized distributions of the tilt angle, $\theta_g$, of BDT molecules from the surface normal.

Figure 8 shows the probability distributions for the first torsion $\phi$ on the top and bridge sites. Basically, these distributions demonstrate 90° torsions of Au−S−C−C bonds, which means that an out-of-plane bending of the benzene ring is favorable. In Figure 8b, results from the large basis set show some divergence because the torsion force constant from ab initio calculations with a large basis set is 2 times smaller than that from small-basis calculations (Table 3). The second torsion curves $\psi$ on the bridge site show some interesting phenomena (Figure 9). Whereas both MD and Boltzmann factor distributions from the two basis sets find two peaks at $\psi = 0$ and 180°, which means that the S−C bond tilting toward the bridge Au atoms is favorable, there are also two additional peaks at 50 and 130° (small basis) or 25 and 155° (large basis) in the MD distributions. The total area enveloped by the small peaks is about $^1/_3$ (the total probability of the normalized distribution equals unity), implying that $^1/_3$ of bridge BDT molecules have to rotate their Au−SC−S8−C4 dihedral angles to form a global herringbone structure (Figure 5a). In Figure 1, there are three kinds of bridge sites on the Au(111) surface, depending on their Au−Au bridge orientation: 0, 60, and 120°. It turns out that the BDT molecules residing on 120° sites undergo such rotation.

**C. Global Molecular Orientations.** The above results and discussions on the local BDT−Au bonding show that the nonbonded intermolecular interactions also play an important role in BDT−Au binding. We now consider the global molecular orientations, which can be described by three angles (Figure 10): the tilt angle from the Au(111) surface normal, $\theta_g$; the azimuthal angle $\chi$, which defines the tilt direction of BDT molecules relative to the $x$ axis; and the twist angle $\psi_g$, which defines the rotation of the benzene ring around the BDT molecular axis (which is 0° when the surface normal ($z$ axis) and benzene ring are in the same plane). These global geometric parameter distributions are shown in Figure 11 to Figure 13. It can be seen clearly that whereas the local bonding geometry may depend on the selected basis set this dependence is not significant for the global molecular orientations. The peak differences in probability distributions are well within 15%

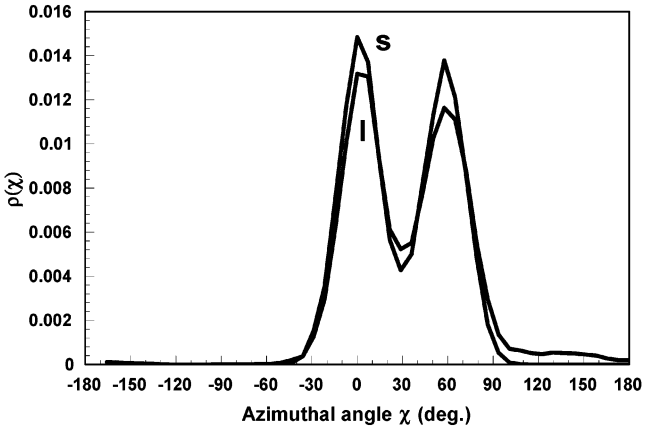


**Figure 12.** Normalized distributions of the azimuthal angle, $\chi$, of BDT molecules from the *x* axis.

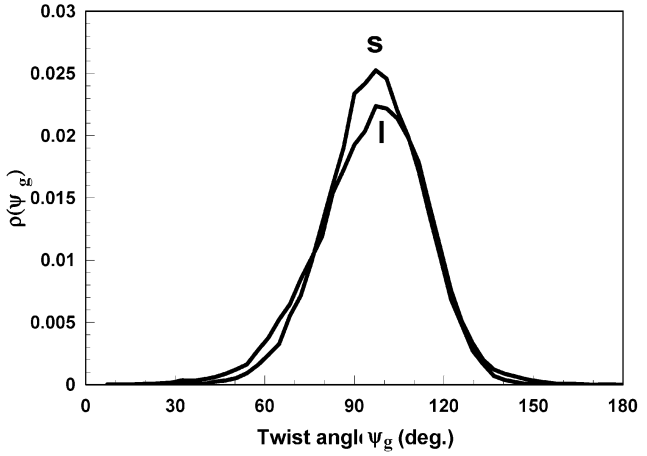


**Figure 13.** Normalized distributions of the twist angle, $\psi_g$, of BDT molecules. When the *z* axis and benzene ring are in the same plane, $\psi_g = 0$.

because the overall global structure of BDT SAMs is largely determined by the steric constraints between BDT molecules. In Figure 11, both basis sets give a tilt angle of around 26°, which is comparable to that of BT molecules on a Au(111) surface[24,44] and is also comparable to that of alkylthiols on a Au(111) surface.[45] The azimuthal angle distribution in Figure 12 presents two peaks at $\chi = 0$ and 60°, corresponding to the two tilt directions in the herringbone structure of BDT molecules. These two tilt directions, in fact, are basically along the two bridge Au directions of 0 and 60°, which can also be seen in Figure 5a. In Figure 13, the twist angles, $\psi_g$, predicted from the two basis sets are approximately 95° (out-of-plane tilting), which is also comparable to that in the experiment pertaining to BT molecules on a Au(111) surface.[24] These $\psi_g$ distributions are very similar to those local torsion distributions in Figure 8 that are due to the rigidity of benzene rings in BDT molecules.

## VI. Conclusions

The binding picture presented in this paper of a benzenedithiol (BDT) self-assembled monolayer on a Au(111) surface shows that it is possible to provide a pathway to the large-scale modeling of molecular electronics devices. Because accurate predictions of binding properties at the molecule−metal interface and molecular configuration are important to subsequent conductance and electron-transport calculations, the development of accurate force fields and highly efficient computational tools is crucial. This in turn provides guidance to electronics architectural design. We show that by using the universal force field (UFF),[15] combined with BDT−Au bonding potentials developed from ab initio calculations[16−18,28] and molecular dynamics strategies described in this paper, the structure of BDT molecules on a gold surface can be well defined. The predicted structure parameters, for example, the tilt and twist angles of BDT molecules are similar to those that were experimentally measured for BT molecules on Au(111) surfaces. The predicted herringbone structure needs further experimental verification, possibly from neutron-scattering experiments.

**Acknowledgment.** We thank P. S. Krstic, D. J. Dean, and J. C. Wells at Oak Ridge National Laboratory (ORNL) for providing details of the ab initio calculations characterizing the BDT−Au interaction, which were needed to implement molecular dynamics simulations. This work was supported by the Laboratory Directed Research and Development (LDRD) program at ORNL, managed by UT-Battelle for the U.S. Department of Energy under contract no. DE-AC05-00OR 22725.

## Appendix: Numerical Procedure in Double RESPA

In the seminal work of Tuckerman et al.,[26] the Liouville operator corresponding to the pseudo-Hamiltonian (eq 3-1) is given by

$$iL = \dot{x}\frac{\partial}{\partial x} + [F(x) - \dot{\eta}p]\frac{\partial}{\partial p} + \dot{\eta}\frac{\partial}{\partial \eta} + F_\eta(p)\frac{\partial}{\partial p_\eta} \quad \text{(A-1)}$$

where

$$F(x) = -\frac{\partial V}{\partial x}$$

and

$$F_\eta(p) = \sum \frac{p^2}{m} - 3NkT$$

If we decompose the total force $F(x)$ into the short-range force $F_s(x)$ (the intramolecular interaction) and the long-range force $F_l(x)$ (the intermolecular interaction) and define the reference system operator as

$$iL_r = \dot{x}\frac{\partial}{\partial x} + F_s(x)\frac{\partial}{\partial x}$$

then eq A-1 becomes

$$iL = iL_r + F_l(x)\frac{\partial}{\partial p} - \dot{\eta}p\frac{\partial}{\partial p} + \dot{\eta}\frac{\partial}{\partial \eta} + F_\eta(p)\frac{\partial}{\partial p_\eta} = iL_r + iL_1 \quad \text{(A-2)}$$

where $iL_1$ is the remaining operator.

Suppose that $\Gamma(0) = \Gamma(x(0), p(0), \eta(0), p_\eta(0))$ is the initial state of the molecular system. The state of the system at time *t* is given by

$$\Gamma(t) = e^{iLt}\Gamma(0) \quad \text{(A-3)}$$

For a small time step $\Delta t$, the propagator $e^{iL\Delta}t$ can be factored using the Trotter theorem as[26]

$$e^{iL\Delta t} = e^{iL_1\Delta t/2}e^{iL_r\Delta t}e^{iL_1\Delta t/2} \quad \text{(A-4)}$$

The middle propagator in eq A-4 involves the calculation of short-range forces that have fast varying characteristics with

large magnitudes. This will need a smaller time step $\delta t = \Delta t/n$ to integrate the equations of motion in the reference system for $n$ times.

In our BDT−Au system, we find that by using the single RESPA the average displacement of H atoms for a smaller time step $\delta t$ is always quite a bit larger than those of C and S atoms because of the disparate mass problem, resulting in a drift in total energy $H'$. Tuckerman et al.[26] suggested a double-RESPA algorithm that involves updates of the long-range force for light particles. As discussed before, it seems that this is not an optimal algorithm for BDT molecules. We propose an alternative approach that directly decomposes the propagator for light particles within the reference system. We rewrite the reference system operator as

$$iL_r = iL_{xr} + iL_{yr}$$

$$iL_{xr} = \dot{x}\frac{\partial}{\partial x} + F_{xs}(x,y)\frac{\partial}{\partial p_x} \qquad iL_{yr} = \dot{y}\frac{\partial}{\partial y} + F_{ys}(x,y)\frac{\partial}{\partial p_y} \tag{A-5}$$

where $x$ and $y$ label fast and slow degrees of freedom. Then the middle propagator in eq A-4 can be written as

$$e^{iL_r\Delta t} = [e^{iL_{xr}(\delta t/2)}e^{iL_{yr}\delta t}e^{iL_{xr}(\delta t/2)}]^n \qquad (\Delta t = n\delta t) \tag{A-6}$$

In the above equation, a second decomposition is employed in the propagator $e^{iL_{xr}(\delta t/2)}$, yielding

$$e^{iL_{xr}(\delta t/2)}e^{iL_{yr}\delta t}e^{iL_{xr}(\delta t/2)} = [e^{iL_{xr}(dt)}]^{m/2}e^{iL_{yr}\delta t}[e^{iL_{xr}(dt)}]^{m/2} \qquad (\delta t = mdt) \tag{A-7}$$

where

$$e^{iL_{xr}(dt)} = e^{(dt/2)F_{xs}(x,y)\partial/\partial p_x}e^{dt\,\dot{x}\partial/\partial x}e^{(dt/2)F_{xs}(x,y)\partial/\partial p_x} \tag{A-8}$$

$$e^{iL_{yr}\delta t} = e^{(\delta t/2)F_{ys}\partial/\partial p_y}e^{\delta t\,\dot{y}\partial/\partial y}e^{(\delta t/2)F_{ys}\partial/\partial p_y} \tag{A-9}$$

The total gain of this double-RESPA scheme is $mn$.

Consider the initial state of the molecular system $\Gamma(0) = \{x(0), y(0), p_x(0), p_y(0), \eta(0), p_\eta(0)\}$ and the new state $\Gamma(\Delta t)) = \{x(\Delta t), y(\Delta t), p_x(\Delta t), p_y(\Delta t), \eta(\Delta t), p_\eta(\Delta t)\}$ at time $\Delta t$, where $x$ and $y$ are the coordinates of the light and heavy particles, $p_x$ and $p_y$ are the corresponding conjugated momenta, and $\eta$ and $p_\eta$ are the thermostat coordinate and momentum. From ref 26, we know that the third propagator $e^{iL_1\Delta t/2}$ in eq A-4 propagates the phase variables to

$$x(0) \rightarrow x_0 = x(0)$$

$$y(0) \rightarrow y_0 = y(0)$$

$$p_x(0) \rightarrow p_{x0} = \left[p_x(0) + \frac{\Delta t}{4}F_l(0)\right]e^{-(\Delta t/2)((p_{\eta 0})/Q)} + \frac{\Delta t}{4}F_l(0)$$

$$p_y(0) \rightarrow p_{y0} = \left[p_y(0) + \frac{\Delta t}{4}F_l(0)\right]e^{-(\Delta t/2)((p_{\eta 0})/Q)} + \frac{\Delta t}{4}F_l(0)$$

$$\eta(0) \rightarrow \eta_0 = \eta(0) + \frac{\Delta t}{2}\frac{p_{\eta 0}}{Q}$$

$$p_\eta(0) \rightarrow p_{\eta 0} = p_\eta(0) + \frac{\Delta t}{2}F_\eta(0)$$

where $F_l(0) = F_l(x(0), y(0))$ is the initial long-range force and $F_\eta(0) = \sum p^2(0)/m\text{-}3NkT$ is the initial thermostat force.

The middle propagator $e^{iL_r\Delta t}$ in eq A-4 can be further decomposed according to eqs A-6−A-9, which propagates only the coordinates and momenta of all of the particles and generates a velocity Verlet algorithm in the reference system:

$$\left.\begin{aligned} x_0 &\rightarrow x_0 + dt\left(\frac{p_{x_0}}{m}\right) + \frac{1}{2}(dt)^2\frac{F_{xs}(x_0,y_0)}{m} = x(dt) \\ p_{x0} &\rightarrow p_{x0} + \frac{dt}{2}[F_{xs}(x_0,y_0) + F_{xs}(x(dt),y_0)] \end{aligned}\right\}$$

integrate $^m/_2$ time steps $dt$ (A-10)

$$\left.\begin{aligned} y_0 &\rightarrow y_0 + \delta t\frac{p_{y_0}}{m} + \frac{1}{2}(\delta t)^2\frac{F_{ys}\left(x\left(\frac{\delta t}{2}\right),y_0\right)}{m} = y(\delta t) \\ p_{y_0} &\rightarrow p_{y_0} + \frac{\delta t}{2}\left[F_{ys}\left(x\left(\frac{\delta t}{2}\right),y_0\right) + F_{ys}\left(x\left(\frac{\delta t}{2}\right),y(\delta t)\right)\right] \end{aligned}\right\}$$

integrate one time step $\delta t$ (A-11)

$$\left.\begin{aligned} x\left(\frac{\delta t}{2}\right) &\rightarrow x\left(\frac{\delta t}{2}\right) + dt\frac{p_{x_0}\left(\frac{\delta t}{2}\right)}{m} + \frac{1}{2}(dt)^2\frac{F_{xs}\left(x\left(\frac{\delta t}{2}\right),y(\delta t)\right)}{m} \\ p_x\left(\frac{\delta t}{2}\right) &\rightarrow p_x\left(\frac{\delta t}{2}\right) + \frac{dt}{2}\left[F_{xs}\left(x\left(\frac{\delta t}{2}\right),y(\delta t)\right) + F_{xs}\left(x\left(\frac{\delta t}{2}+dt\right),y(\delta t)\right)\right] \end{aligned}\right\}$$

integrate $^m/_2$ time steps $dt$ (A-12)

where $\delta t = m(dt)$. Then, repeat the integration processes A-10−A-12 $n$ times to $\Delta t$.

Now the coordinates of all of the light and heavy particles have been propagated to $\{x(\Delta t), y(\Delta t)\}$, but their momenta $\{p_x, p_y\}$ need to be propagated by the long-range forces $F_l$ from the current state $\{p_{xr}(\Delta t; x(\Delta t), y(\Delta t), p_{x0}(\Delta t)), p_{yr}(\Delta t; x(\Delta t), y(\Delta t), p_{y0}(\Delta t))\}$ to the final state $\{p_x(\Delta t), p_y(\Delta t)\}$. This is done by the first propagator in eq A-4, which yields

$$p_x(\Delta t) = \left\{p_{xr}(\Delta t; x(\Delta t), y(\Delta t), p_{x0}(\Delta t)) + \frac{\Delta t}{4}F_l(\Delta t)\right\} \times e^{-(\Delta t/2)((p_{\eta 0})/Q)} + \frac{\Delta t}{4}F_l(\Delta t)$$

$$p_y(\Delta t) = \left\{p_{yr}(\Delta t; x(\Delta t), y(\Delta t), p_{y0}(\Delta t)) + \frac{\Delta t}{4}F_l(\Delta t)\right\} \times e^{-(\Delta t/2)((p_{\eta 0})/Q)} + \frac{\Delta t}{4}F_l(\Delta t)$$

The thermostat coordinate $\eta$ and momenta $p_\eta$ are finally propagated to

$$\eta(\Delta t) = \eta_0 + \frac{\Delta t}{2}\frac{p_{\eta_0}}{Q} = \eta(0) + \frac{\Delta t p_\eta(0)}{Q} + \frac{\Delta t^2}{2Q}F_\eta(0)$$

$$p_\eta(\Delta t) = p_{\eta_0} + \frac{\Delta t}{2}F_\eta(\Delta t) = p_\eta(0) + \frac{\Delta t}{2}[F_\eta(0) + F_\eta(\Delta t)]$$

## References and Notes

(1) Proceedings of a Conference on Molecular Electronics: Science and Technology, December 14−18, 1997, Humacao, Puerto Rico 1998; Aviram, A.; Ratner, M.; Eds.; *Ann. N.Y. Acad. Sci.* **1998**, *852*.

(2) Aviram, A.; Ratner, M. A. *Chem. Phys. Lett.* **1974**, *29*, 277.

(3) Joachim, C.; Gimzewski, J. K.; Aviram, A. *Nature (London)* **2000**, *408*, 541.

(4) Chen, J.; Reed, M. A.; Rawlett, A. M.; Tour, J. M. *Science (Washington, D.C.)* **1999**, *286*, 1550.

(5) Reed, M. A.; Zhou, C.; Muller, C. J.; Burgin, T. P.; Tour, J. M. *Science (Washington, D.C.)* **1997**, *278*, 252.

(6) Seminario, J. M.; Zacarias, A. G.; Tour, J. M. *J. Phys. Chem. A* **1999**, *103*, 7883.

(7) Di Ventra, M.; Pantelides, S. T.; Lang, N. D. *Phys. Rev. Lett.* **2000**, *84*, 979.
(8) Samanta, M. P.; Tian, W.; Datta, S.; Henderson, J. I.; Kubiak, C. P. *Phys. Rev. B* **1996**, *53*, R7626.
(9) Kornilovitch, P. E.; Bratkovsky, A. M. *Phys. Rev. B* **2001**, *64*, 195413.
(10) Xue, Y. Q.; Datta, S.; Ratner, M. A. *J. Chem. Phys.* **2001**, *115*, 4292.
(11) Di Ventra, M.; Kim, S. G.; Pantelides, S. T.; Lang, N. D. *Phys. Rev. Lett.* **2001**, *86*, 288.
(12) Hipps, K. W. *Science (Washington, D.C.)* **2001**, *294*, 536.
(13) Yaliraki, S. N.; Kemp, M.; Ratner, M. A. *J. Am. Chem. Soc.* **1999**, *121*, 3428.
(14) Cui, X. D.; Primak, A.; Zarate, X.; Tomfohr, J.; Sankey, O. F.; Moore, A. L.; Moore, T. A.; Gust, D.; Harris, G.; Lindsay, S. M. *Science (Washington, D.C.)* **2001**, *294*, 571.
(15) Rappé, A. K.; Casewit, C. J.; Colwell, K. S.; Goddard, W. A.; Skiff, W. M. *J. Am. Chem. Soc.* **1992**, *114*, 10024.
(16) The ab initio calculations and all of the related data necessary for fitting BDT−Au potentials were provided by P. S. Krstic, D. J. Dean, and J. C. Wells at Oak Ridge National Laboratory (ORNL) using the NWChem package. For a description of NWChem, see Bernholdt, D. E.; Apra, E.; Fruchtl, H. A.; Guest, M. F.; Harrison, R. J.; Kendall, R. A.; Kutteh, R. A.; Long, X.; Nicholas, J. B.; Nichols, J. A.; Taylor, H. L.; Wong, A. T. *Int. J. Quantum Chem.* **1995**, Suppl. *29*, 475.
(17) Krstic, P. S.; Dean, D. J.; Zhang, X. G.; Keffer, D.; Leng, Y. S.; Cummings, P. T.; Wells, J. C. *Comput. Mater. Sci.*, in press, 2003.
(18) Keffer, D. J.; Krstic, P. S.; Leng, Y. S.; Dean, D. J.; Wells, J. C.; Cummings, P. T., in preparation.
(19) Sellers, H.; Ulman, A.; Shnidman, Y.; Eilers, J. E. *J. Am. Chem. Soc.* **1993**, *115*, 9389.
(20) Beardmore, K. M.; Kress, J. D.; Gronbech-Jensen, N.; Bishop, A. R. *Chem. Phys. Lett.* **1998**, *286*, 40.
(21) Gronbeck, H.; Curioni, A.; Andreoni, W. *J. Am. Chem. Soc.* **2000**, *122*, 3839.
(22) Gottschalck, J.; Hammer, B. *J. Chem. Phys.* **2002**, *116*, 784.
(23) Yourdshahyan, Y.; Rappé, A. M. *J. Chem. Phys.* **2002**, *117*, 825.
(24) Wan, L. J.; Terashima, M.; Noda, H.; Osawa, M. *J. Phys. Chem. B* **2000**, *104*, 3563.
(25) Leng, Y. S.; Jiang, S. Y. *J. Am. Chem. Soc.* **2002**, *124*, 11764.
(26) Tuckerman, M.; Berne, B. J.; Martyna, G. J. *J. Chem. Phys.* **1992**, *97*, 1990.
(27) Yeh, I. C.; Berkowitz, M. L. *J. Chem. Phys.* **1999**, *111*, 3155.
(28) Krstic, P. S.; Dean, D. J.; Wells, J. C. Personal communications. Currently, the density functionals used in ab initio calculations are the local density approximation (LDA) with Slater exchange and Vosko−Wilk−Nusair (VWN-V) correlation functionals. The two Gaussian basis sets are the 3-21G and 6-311G for C, S, and H in the BDT molecule, and the effective core potential (ECP) is used for the Au atom. (For the Au atoms with 79 electrons per atom, a frozen-core approximation represents all electrons except for those in the outmost orbitals. In the small basis set, the 68 core electrons are represented by ECP, and the remaining 11 active electrons are represented by 10 basis functions. Whereas in the large basis set the ECP potential represents 60 core electrons of Au, and the remaining 19 active electrons are represented by 44 functions). Further investigations using the PBE0 functional (a hybrid, parameter-free approximation for exchange-correlation combining a generalized gradient functional (LDA-GGA)) will be published in a separate paper (ref 18). It is noted that in recent calculations Larsson et al.[29] used the LDA-B3-LYP functional rather than the PBE functional for thiol molecular linkers on the $Au_{13}$ cluster.
(29) Larsson, J. A.; Nolan, M.; Greer, J. C. *J. Phys. Chem. B* **2002**, *106*, 5931.
(30) Nosé, S. *J. Chem. Phys.* **1984**, *81*, 511.
(31) Hoover, W. G. *Phys. Rev. A* **1985**, *31*, 1695.
(32) Martyna, G. J.; Klein, M. L.; Tuckerman, M. *J. Chem. Phys.* **1992**, *97*, 2635.
(33) Martyna, G. J.; Tuckerman, M. E.; Tobias, D. J.; Klein, M. L. *Mol. Phys.* **1996**, *87*, 1117.
(34) Parry, D. E. *Surf. Sci.* **1975**, *49*, 433.
(35) Heyes, D. M.; Barber, M.; Clarke, J. H. R. *J. Chem. Soc., Faraday Trans. 2* **1977**, *73*, 1485.
(36) Deleeuw, S. W.; Perram, J. W. *Mol. Phys.* **1979**, *37*, 1313.
(37) Deleeuw, S. W.; Perram, J. W.; Smith, E. R. *Proc. R. Soc. London, Ser. A* **1980**, *373*, 27.
(38) Allen, M. P.; Tildesley, D. J. *Computer Simulation of Liquids*; Oxford University Press: New York, 1987.
(39) Spohr, E. *J. Chem. Phys.* **1997**, *107*, 6342.
(40) Smith, E. R. *Proc. R. Soc. London, Ser. A* **1981**, *375*, 475.
(41) Grzybowski, A.; Brodka, A. *Mol. Phys.* **2002**, *100*, 1017.
(42) Minary, P.; Tuckerman, M. E.; Pihakari, K. A.; Martyna, G. J. *J. Chem. Phys.* **2002**, *116*, 5351.
(43) Arnold, A.; de Joannis, J.; Holm, C. *J. Chem. Phys.* **2002**, *117*, 2496.
(44) Jung, H. H.; Do Won, Y.; Shin, S.; Kim, K. *Langmuir* **1999**, *15*, 1147.
(45) Hautman, J.; Klein, M. L. *J. Chem. Phys.* **1989**, *91*, 4994.
(46) Mahaffy, R.; Bhatia, R.; Garrison, B. J. *J. Phys. Chem. B* **1997**, *101*, 771.